Available online at www.sciencedirect.com

SciVerse ScienceDirect

Ceramics International 39 (2013) 2293–2302

CERAMICS INTERNATIONAL

www.elsevier.com/locate/ceramint

Effect of arc current on microstructure, texturing and wear behavior of plasma sprayed $CaZrO_3$ coatings

M. Khalid[a,*], M. Mujahid[a], A. Nusair Khan[b], R.S. Rawat[c], K. Mehmood[b]

[a]School of Chemical and Materials Engineering, National University of Sciences and Technology, Sector H-12, Islamabad, Pakistan
[b]Institute of Industrial Control Systems, Rawalpindi, Pakistan
[c]NSSE, National Institute of Education, Nanyang Technological University, Singapore

Received 19 July 2012; received in revised form 14 August 2012; accepted 26 August 2012
Available online 1 September 2012

Abstract

In order to enhance the biocompatibility of metallic implants, various ceramic coatings are currently in vogue. $CaZrO_3$, a promising candidate material, was deposited through plasma spraying on stainless steel (316L) substrates at arc currents of 400, 500 and 600 A. The coatings were characterized using a SEM, XRD, surface profilometers and a tribometer. It was found that the arc current had profound effects on the thickness, microstructure, phase evolution, crystallinity and wear behavior of the coatings. The cross-sectional images and fractographic analysis showed that a denser coating with better inter-splat fusion was produced at arc current of 600 A. The average roughness (Ra) of the coatings increased from 3.62 to 6.68 μm as the arc current was increased from 400 to 600 A. The feedstock (powder) and the coatings were predominantly composed of $CaZrO_3$ along with a minor amount of $CaZr_4O_9$ phase. The rise in the arc current resulted in a slight increase in the relative proportion of the $CaZrO_3$ phase. Also, the coating produced at arc current of 600 A exhibited highest crystallinity. The detailed XRD analysis of (002) and (200) reflections of the ferroelectric $CaZrO_3$ revealed the preferred orientation of crystals in the coatings. The presence of this texture is explained on the basis of shifting the unstable Zr^{4+} ion in oxygen octahedral cage preferably in one direction. The increase in the arc current decreased the coefficient of friction and, as a result, relatively better wear resistance was observed for the coating produced using higher arc current. Moreover, the coating fabricated using arc current of 600 A reduced the volumetric weight loss by 13 times during the wear test as compared to the substrate. Plasma sprayed $CaZrO_3$ coating not only enhanced the wear resistance of the stainless steel but also showed the potential to furnish a bioactive surface.

Keywords: C. Wear resistance; Plasma spraying; $CaZrO_3$; Texturing

1. Introduction

Stainless steel (316L) is widely used in various orthopedic devices/implants such as fracture plates, screws, nails, prostheses for total hip replacements and dental roots [1] due to its low cost, availability, ease of processing and good corrosion resistance. The exposure of implants to human tissues and fluids results in its wear and corrosion [2,3] ultimately leading to its failure. The corrosion products from SS316L (especially concentration of Ni above 11.7 ppm) were found to be toxic in *in vitro* studies [4,5]. Metal ion release from the implants is another complication that has raised concerns for the health care professionals [6–8]. For enhanced biocompatibility, metallic implants are coated with calcium phosphates, especially, hydroxyapatite (HA). These coatings not only make the surfaces conducive for osseointegration but also act as a barrier to diffusion of the harmful metallic elements into the body. In one study, metal ions released from HA coated Ti_6Al_4V alloy were substantially reduced by the use of 200 μm thick HA coating as compared to 50 μm thick coating [8]. However, these coatings are not perfect; delamination and/or dissolution of the coatings is reported in many *in vivo* and *in vitro* studies [9–11]. Degradation of the metal implants and coatings may also occur by abrasion/wear during the insertion of the implants into the organs or through the micro-movements between bone/cement and metal alloy. The wear due to micro-movements is expected to increase when the

*Corresponding author. Tel.: +92 333 561 44 66.
E-mail address: semelkhalid@hotmail.com (M. Khalid).

0272-8842/$ - see front matter © 2012 Elsevier Ltd and Techna Group S.r.l. All rights reserved.
http://dx.doi.org/10.1016/j.ceramint.2012.08.076

implant loosens. Aseptic loosening (osteolysis) has been a major cause of implant failures. The components in the surgical field that experience abrasion include femoral stems, external fixation pins, pedicle screws for spine stabilization, root-form endosseous dental implants, etc. [12]. In this regard, the fretting wear behavior of HA coatings and composites is widely studied [13–15].

To increase the mechanical stability of the coatings, efforts are being made to improve their fracture toughness and wear resistance by reinforcing them with carbon nanotubes [16–18]. Laser surface treatment has also been found effective for increasing the wear and corrosion resistance of SS316L steel [19]. Apart from improving the mechanical properties of HA coatings, researchers are also working on alternatives to HA which are bioactive (CaO–ZrO_2–SiO_2, nanostructured ZrO_2) [20,21] and wear resistant (ZrO_2, Al_2O_3–13%TiO_2) [22].

ZrO_2 is a known bio-inert [23] ceramic that could be partially or fully stabilized with CaO, MgO and Y_2O_3 to increase its fracture toughness. In present investigation, the material used for coatings is $CaZrO_3$. It is formed when ZrO_2 is stabilized with 31 wt% CaO as per the phase diagram described in the paper by Stubican and Ray [24]. Plasma sprayed ZrO_2 and calcia stabilized zirconia (CSZ) coatings on metallic substrates have already been investigated for their applications in orthopedics [21,25,26]. Wang et al. prepared CaO stabilized (12.8, 16, 30 mol%) ZrO_2 coatings and showed that the bioactivity of the coatings decreased as the CaO content increased [26]. The CSZs (including $CaZrO_3$) have also been investigated for their possible use as thermal barrier coatings for aero-engines due to their high melting points and low thermal conductivities [27,28]. To the best of our knowledge, the wear behavior of plasma sprayed $CaZrO_3$ coatings has not been reported yet.

$CaZrO_3$, an intermediate compound in CaO–ZrO_2 system, is a ferroelectric ceramic [29] having high dielectric constant (32) and low loss tangent which makes it suitable for multilayer capacitors and resonators [30]. Being a ferroelectric ceramic, a positive or negative charge could be produced on its surface depending upon the direction of polarization during poling by electrical field and this charge can be utilized to enhance the apatite deposition. It has been reported that the negatively charged surfaces of ceramics like $BaTiO_3$ and HA enhance apatite precipitation on exposure to the physiological environment [31–33]. A negatively charged surface of poling treated $BaTiO_3$ ceramic has been shown to deposit calcium phosphate *in vitro* [32]. Also, the negative charge created by electrical polarization on HA surface accelerated the osteobonding in canine bone tissues [31].

In present study, the $CaZrO_3$ coatings have been deposited on SS 316L substrates using atmospheric plasma spraying to evaluate the effect of arc current on the microstructure, texturing and wear behavior of the coatings.

2. Experimental

2.1. Atmospheric plasma spraying of $CaZrO_3$ on SS316L substrates

Austenitic stainless steel (316L) coupons, diameter 25 and 5 mm thickness, were coated with $CaZrO_3$ using an atmospheric plasma spraying apparatus (Sulzer Metco 3MB Gun). The coupons were fixed on a cylinder rotating at 128 rpm during the coating process. The plasma gun was moved horizontally at a speed of 12 mm/s while the substrates were cooled by air blast during the spraying process. Before coating, the coupons were grit blasted with brown alumina (#46) at an angle of 90° and a pressure of 80 psi. This was followed by cleaning the coupon surface with air blast to remove debris. A schematic diagram of the coating process is shown in Fig. 1. The process parameters for plasma spraying are given in Table 1. The coatings were prepared at arc currents of 400, 500 and 600 A while keeping other parameters constant.

2.2. Characterization of powder and coatings

Surface and cross-sectional morphologies of the coatings were investigated in a Jeol JSM-6490A scanning electron microscope. Cross sectional analysis was also carried out by an optical microscope. Three dimensional topographical mapping was accomplished by a Taylor–Hubson Precision

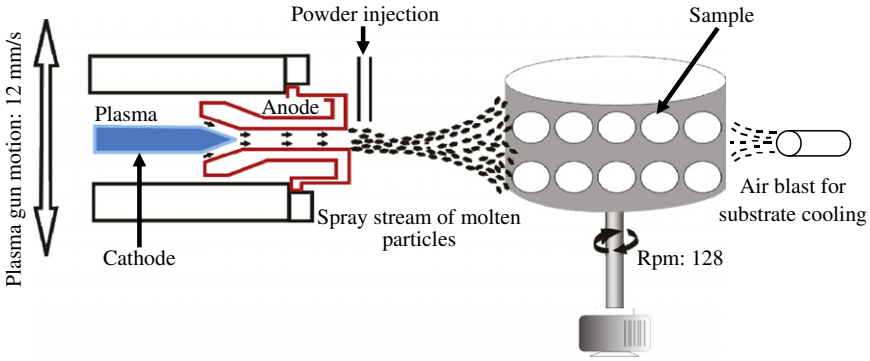

Fig. 1. Schematic representation of the atmospheric plasma spraying process.

Table 1
Process parameters for deposition of $CaZrO_3$ on SS316L substrates by plasma spraying.

Coating parameters	Coating ID		
	C400A	C500A	C600A
Plasma current (A)	400	500	600
Plasma voltage (V)	46	48	50
Plasma gas (Ar) flow (SCFH)		180	
Plasma gas (H_2) flow (SCFH)		20	
Carrier gas (Ar) flow (SCFH)		40	
Feed rate (lb/h)		6	
Stand off distance, (mm)		102	
Number of passes		160	

(Talyscan 150) profilometer in contact mode. The area analyzed was 1 mm × 1 mm with step size of 5 μm. The surface roughness of the coatings was also measured using a two dimensional surface roughness tester (Diavite DH-5) with a resolution of 0.01 μm (Ra). The scanning was carried out in both horizontal as well as in the vertical direction. Each scan was 15 mm in length and an average of eight measurements is quoted. The phase analysis was carried out on a Siemens D5005 X-Ray diffractometer in locked couple mode using Cu-Kα radiation with a scan step size of 0.02° and 3 s dwell time per step. The diffractometer was operated at 40 kV with a gun current of 40 mA. Coefficient of friction and wear loss of the substrate and coatings were measured by ball-on-disc sliding test with a tribometer (CSEM, Switzerland). In this regard, an alumina ball (diameter 6 mm) was slid against the substrate (SS316L) and the coatings ($CaZrO_3$) at a speed of 20 cm/s. The normal force used in this test was 10 N.

3. Results and discussion

3.1. Morphology of the powder and coatings

The SEM image in Fig. 2 shows that the morphology of $CaZrO_3$ powder used for plasma spraying is composed of non-porous, blocky and angular particles of sizes ranging between 5 and 75 μm. Moreover, the sharp edges of the powder particles indicate that it has been prepared through fusion and crushing.

The optical micrographs of the cross-sections of the coatings are shown in Fig. 3 while the coating thickness values are given in Table 2. It can be observed that the coating thickness increased with increasing arc current. This may be attributed to the fact that at higher plasma current, more powder particles are expected to be in the molten/semi-molten state thereby increasing the deposition efficiency. The optical micrographs of the cross-sections of the coatings (Fig. 3) reveal porosity in all prepared coatings.

The coatings architecture was also studied using SEM (Fig. 4). The surface morphology of the coating deposited at lower arc current of 400 A exhibits the presence of unmelted powder particles (encircled in Fig. 4a) indicating that the plasma temperature was relatively low at this arc

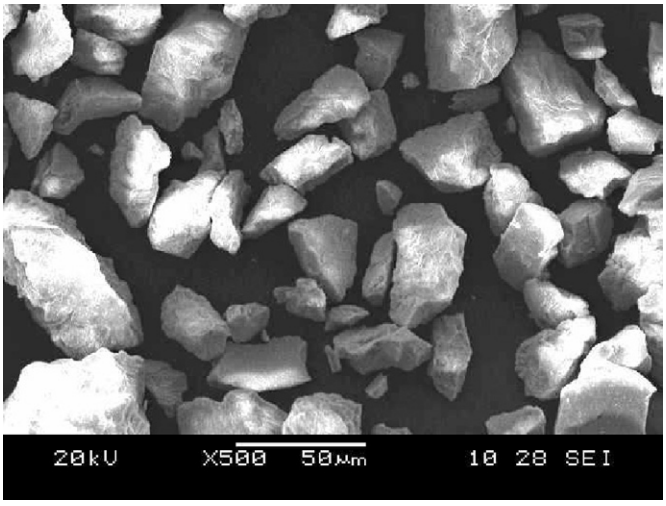

Fig. 2. SEM micrograph of $CaZrO_3$ powder used in plasma spraying.

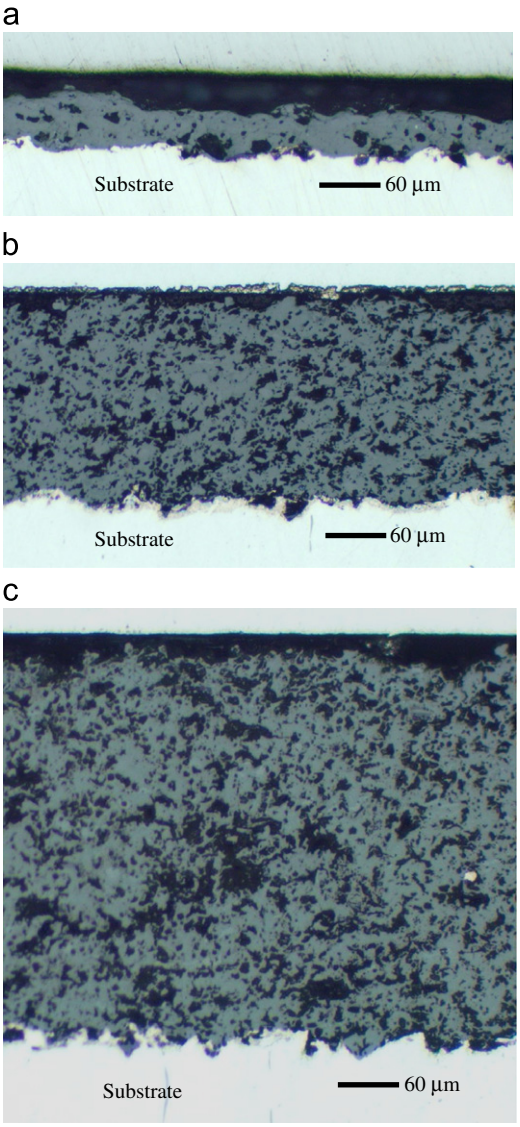

Fig. 3. Optical micrographs of the cross-sections of the coatings sprayed at (a) 400 A, (b) 500 A and (c) 600 A showing that the thickness of the coatings increased with the arc current and presence of porosity in all prepared coatings.

current. The cross-section of the same coating demonstrates relatively high porosity and lack of fusion of the splats, Fig. 4b. On the other hand, the cross-sectional images of the coatings deposited at higher arc currents of 500 and 600 A exhibit lower level of porosity and higher inter-splat fusion compared to the coating deposited at 400 A as shown in Fig. 4b–d.

A comparison between the coatings sprayed at 500 and 600 A shows that the level of porosity is apparently similar but the fusion of splats seems better in case of the coating sprayed at 600 A, refer Fig. 4c and d.

3.2. Fractography of the coatings

Fig. 5 shows the fresh fractured surfaces of all the prepared coatings. It can be noted that the coating sprayed at 400 A has visibly more number of smooth surfaces, Fig. 5a. These smooth surfaces represent porosity in the coating, which upon fracture become revealed. Moreover, it is observed that the development of adequate splats in this coating is poor. This is believed to be due to the lower processing temperatures achieved at low spraying currents.

The coatings sprayed at 500 and 600 A demonstrate almost similar behavior. Both coatings have well developed splats with less porosity, Fig. 5(b and c). However, in case of the coating sprayed at 600 A, cracks are also observed in some splats, Fig. 5c. These cracks may have appeared due to excessive force with which the powder particles struck the substrate at high arc currents. Another reason could be the presence of larger temperature gradient (between the impacting molten particle and substrate) created as a result of higher temperatures achieved by the particles at high operating currents. The quenching of the particles from high temperature, upon reaching the substrate, may induce cracks in the splats.

The average splat thickness measured on the fractographs was 1.89, 1.36 and 1.19 μm for coatings sprayed at 400, 500 and 600 A, respectively. The smaller splat thickness (1.19 μm) for the coating sprayed at 600 A is probably due to the greater degree of melting and flattening of the impacting particles at this current.

Table 2
Surface roughness and thickness of plasma sprayed coatings at various arc currents.

Coating ID	Roughness Ra (μm)		Coating thickness (μm)
	2D profilometer	3D profilometer	
C400A	3.9 ± 0.4	3.62 ± 0.28	55 ± 3
C500A	4.3 ± 0.4	5.88 ± 0.7	192 ± 3
C600A	4.8 ± 0.5	6.68 ± 0.5	300 ± 4

3.3. Roughness of the coatings

Roughness of the implant surface is an important parameter that not only affects the apatite growth and its adhesion

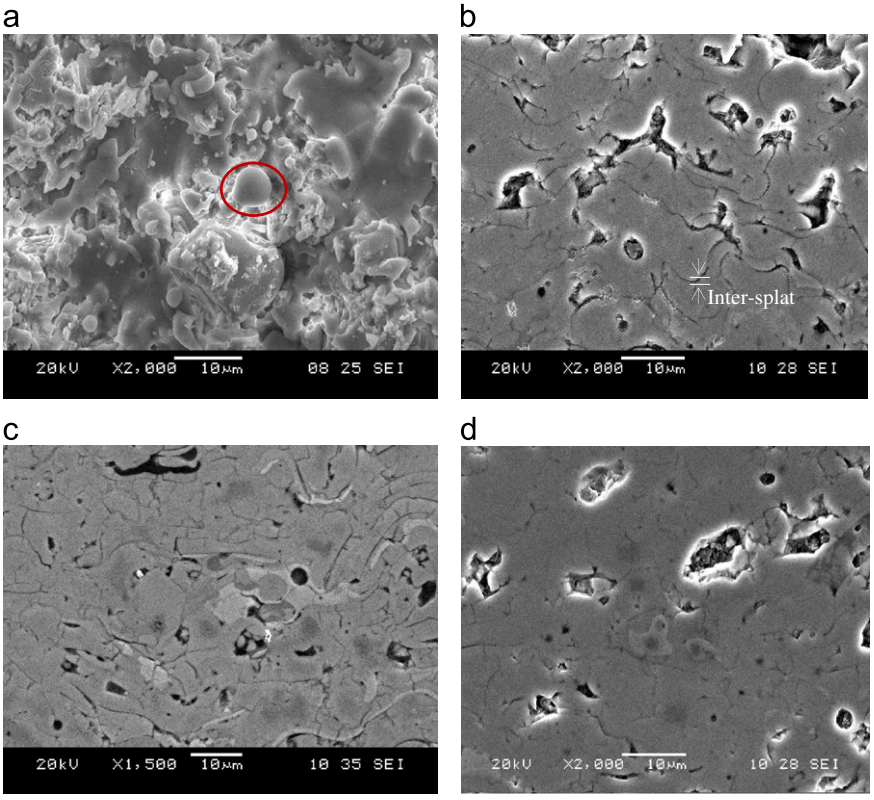

Fig. 4. SEM analysis of the coatings (a) surface of the coatings sprayed at 400 A, indicating the feature (encircled) that the temperature was low (b); (c) and (d) cross-sections of the coating sprayed at 400, 500 and 600 A, respectively. The cross-sectional analysis shows that inter-splat distance decreases with increase in arc current indicating the higher fusion between the splats at higher currents.

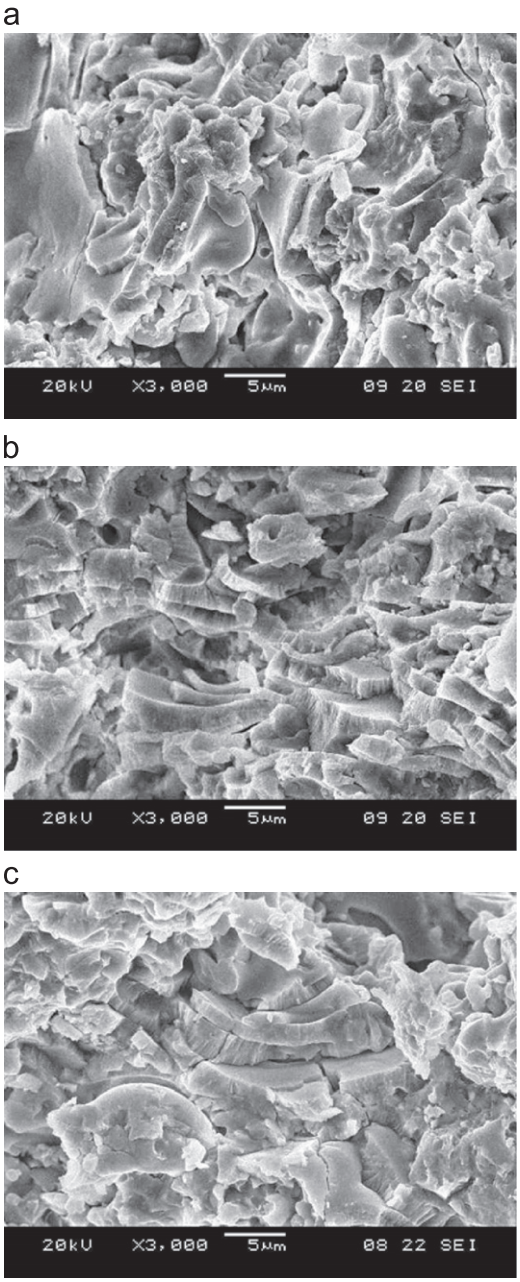

Fig. 5. Fracture morphology of the coatings sprayed at different arc currents: (a) 400 A (b) 500 A and (c) 600 A.

but also influences the wear resistance. High wear rates have been observed between the bone and the metallic alloy in roughened condition as compared to smooth surfaces [34]. Rough implant surfaces might also damage the bone during insertion and cause necrosis. In spite of these disadvantages, increased insertion torque due to rough surface has been found to be beneficial in delaying the loosening of external fixation pins [35]. Furthermore, the rough surfaces of the implants offer greater surface area for tissue–implant interaction. This condition is considered beneficial for enhanced bone apposition [36] as well as for increased shear strength between the bone and the implant *in vivo* [37]. Therefore, roughness of the coating is considered as an important feature for the overall success of such implants.

The surface roughness of the present coatings was measured using both 2D and 3D profilometers. The three-dimensional topographical maps (Fig. 6) demonstrate the presence of rough surfaces on all of the coated samples. The average roughness (Ra) values measured are given in Table 2. It is revealed that Ra value increases with increasing arc current (measured by both 2D and 3D profilometers). However, the Ra values measured with the 3D surface profilometer are relatively higher as compared to the values obtained from the 2D surface profilometer. This may be attributed to the difference in the measurement principles of the two methods. The increase in surface roughness with increase in arc current may be attributed to the higher coating thickness at higher currents (Fig. 3) which is explained as follows. In thermal spraying, the coating is built up by successive stacking of the splats over one another. As the coating thickness increases, the undulations caused by mismatching of the splat boundaries also increase, ultimately resulting in higher roughness. The roughness of the coatings may also affect the wear behavior which is discussed in Section 3.5.

3.4. Phase analysis by XRD

It has been shown that the presence of negative charge on the coatings and bulk ceramics is advantageous to enhance apatite growth *in vivo* [31–33]. The $CaZrO_3$ has a high dielectric constant of about 32 [38] and is expected to provide an appreciable surface charge on its surface. It is also reported that the degree of crystallinity in the coating does affect its stability in the physiological environment i.e. higher crystallinity reduces the dissolution rate [10].

The XRD patterns for $CaZrO_3$ powder and the coatings are shown in Fig. 7. It is revealed that both the powder (feedstock) and the coatings are predominantly composed of the $CaZrO_3$ phase. Minor amounts of the $CaZr_4O_9$ phase are also present as evident from a small peak at $2\theta = 30.08^\circ$. The standard diffraction data cards used for phase identification were 35-0790 and 31-0323 for $CaZrO_3$ and $CaZr_4O_9$, respectively. In the $CaO–ZrO_2$ system, $CaZr_4O_9$ and $CaZrO_3$ phases are formed at 20 and 50 mol% CaO content as mentioned in Ref. [24]. The appearance of $CaZr_4O_9$ phase could be linked to the incomplete reaction between CaO and ZrO_2 during the synthesis of $CaZrO_3$ powder. The $CaZr_4O_9$ phase is a low dielectric constant (10) ceramic and, consequently, a low surface charge is expected on its surface. The relative amount of the two phases ($CaZrO_3$ and $CaZr_4O_9$) in powder and coatings was estimated by calculating the integrated intensity ratio $[I_{(402)}/I_{(121)}]$ in the diffraction peaks from (402) and (121) planes of $CaZr_4O_9$ and $CaZrO_3$ phases, respectively. The degree of crystallinity was also monitored by measuring the broadening and peak height from the (101) diffraction plane of the $CaZrO_3$ phase. The calculated XRD data is given in Table 3. A slight decrease in $I_{(402)}/I_{(121)}$ ratio is observed in the coatings as the arc current is raised. This means that some of the $CaZr_4O_9$ phase is being transformed into the $CaZrO_3$ phase as the arc current is increased. Also, the crystallinity of the powder is higher as compared to the coatings due to the

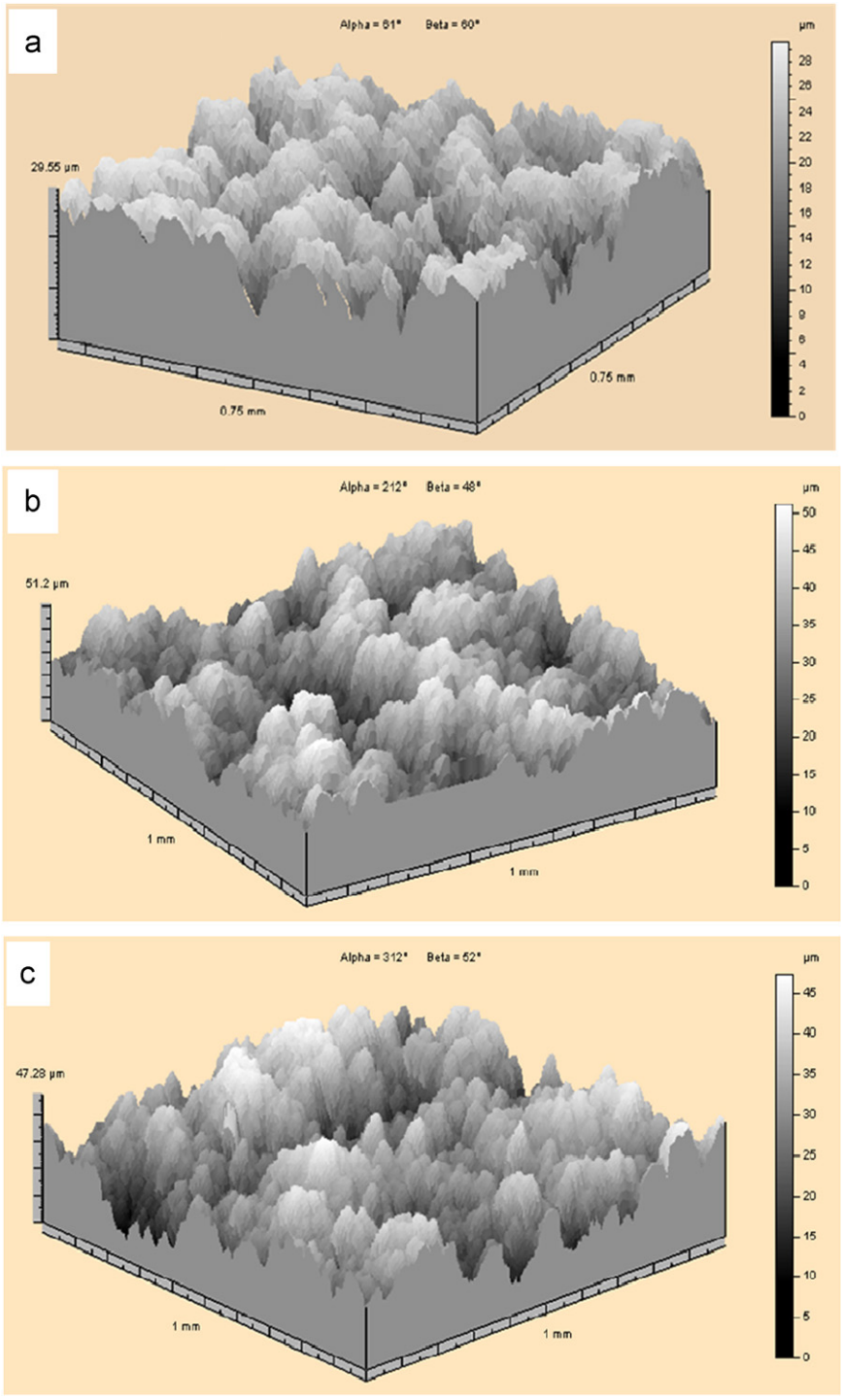

Fig. 6. 3D topographic maps of $CaZrO_3$ coatings sprayed at different arc currents (a) 400 A (b) 500 A and (c) 600 A showing rough surface appearance in all coatings.

fact that the powder would have experienced high cooling rates in plasma spraying which may lead to reduction in crystallinity. Moreover, the coating produced at higher arc current (600 A) is found to be more crystalline than that produced at lower currents (400 and 500 A). Higher crystallinity of the coating prepared at 600 A could be explained on the basis that the splats solidifying in the upper layers of this comparatively thicker coating (thickness 300 μm) may have experienced relatively slow cooling rates that resulted in increased crystallinity. To summarize, the coating produced at 600 A is more crystalline and has slightly larger proportion of high dielectric constant $CaZrO_3$ phase.

An interesting feature in the XRD pattern is observed in $2\theta^{\circ}$ range of 30.5–32.5, see Fig. 7a and its expanded view in Fig. 7b. It can be noticed that for powder the intensity of the (200) plane is higher compared to the (002) plane; however

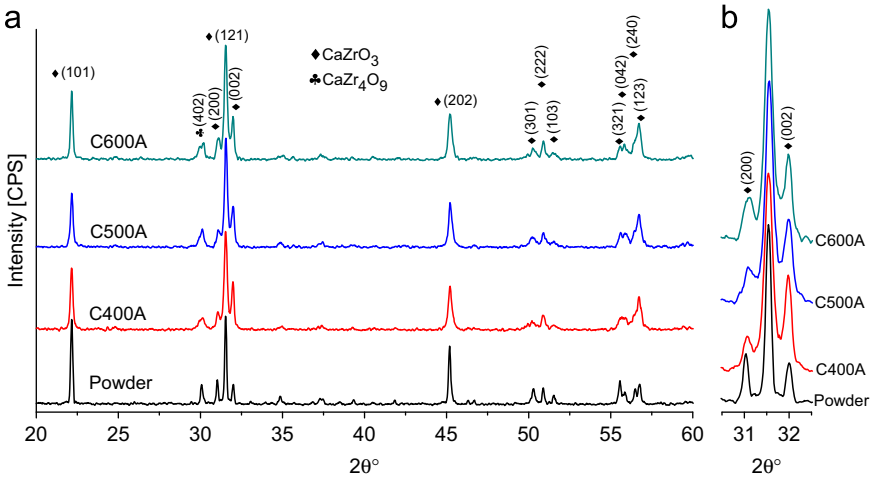

Fig. 7. XRD patterns of $CaZrO_3$ powder and coatings sprayed at various arc currents. From bottom to top: powder, coating sprayed at 400 A, coating sprayed at 500 A and coating sprayed at 600 A (a) in the range $2\theta = 20–60^\circ$ and (b) expanded view in the range $2\theta = 30.5–32.5^\circ$ to highlight the intensities of the planes (200) and (002).

Table 3
Calculated XRD data of $CaZrO_3$ powder and coatings.

	$I_{(402)}/I_{(121)}$	$B_{FWHM(101)}$, 2θ (deg.)	$I_{(101)}$ (a.u.)	$I_{(200)}/I_{(002)}$
Powder	0.224	0.154	134	1.34
C400A	0.206	0.190	95	0.43
C500A	0.200	0.197	80	0.48
C600A	0.174	0.176	103	0.51

for coatings the trend reverses such that now the intensity of the (002) plane is higher compared to the (200) plane. The calculated integrated intensity ratio, $I_{(200)}/I_{(002)}$, for the powder and the coatings is given in Table 3. The observed phenomenon of reversing the reflection intensities could be explained as follows.

$CaZrO_3$ is a ferroelectric ceramic [29] with perovskite structure that has Ca^{2+} ions arranged at the corners of the orthorhombic unit cell while Zr^{4+} ions are placed in the oxygen octahedral cage. Since the size of Zr^{4+} ion is small as compared to surrounding O^{2-} ions [39], it is unstable and may go close to any of the six surrounding O^{2-} ions instead of staying at the center of the octahedral cage, Fig. 8. The off-center position of Zr^{4+} ions causes the polarization of the charges. For this reason, $CaZrO_3$ has a high dielectric constant of about 32 [38]. The area of unit cells in which unstable Zr^{4+} ions are shifted to one crystallographic direction is known as a ferroelectric domain. In ferroelectric ceramics, like $CaZrO_3$, the domains can be switched in one direction (otherwise randomly oriented) by the application of electric or mechanical field, resulting in enhanced polarization in that direction [40].

It has also been observed that the domain switching is accompanied by the appearance of a crystallographic texture. This texture can be evaluated by XRD analysis by measuring the intensities of the reflections of the (200) and (002) planes as evidenced in lead zirconate titanate (PZT) ceramics

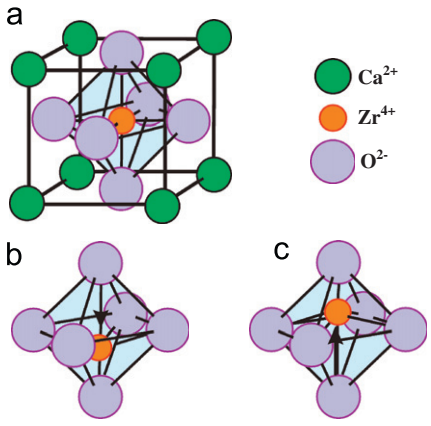

Fig. 8. Schematic of $CaZrO_3$ unit cell (a) showing the position of Zr^{4+} ion at the center of oxygen octahedra. Shifting of the central ion in (b) downward and (c) upward position that produces a charge on the surface.

[41–43]. Hammer et al. [41] reported that the intensity ratio $[I_{(002)}/I_{(200)}]$ was 0.44 for PZT sintered ceramic before poling i.e. in un-textured condition. This intensity ratio increased to 1.86, 1.75 and 1.36 when the ceramic pellets were subjected to mechanical load by cutting, grinding with 220 # SiC paper and grinding with 1000 # SiC paper, respectively. Domains switching has also been observed by XRD in Sr-doped PZT ceramic by applying electrical field in the range of 1–2 kV/mm [42]. In present study, the intensity ratio $[I_{(200)}/I_{(002)}]$ of the $CaZrO_3$ phase of the powder was 1.20, which is close to its value given in JCPDS card no. 35-0790. When the powder is sprayed at 600 A, the said ratio decreases to 0.51. It means that plasma sprayed $CaZrO_3$ coating produced at this current is highly textured, with a preferred orientation along the (002) plane. This corresponds to the condition (in ferroelectric ceramics) as if the domain switching has actually occurred. Upon decreasing the arc current to 500 and 400 A, a slight decrease in the intensity ratio $[I_{(200)}/I_{(002)}]$ to 0.48 and 0.43, respectively, is observed. The highly

textured state in the coatings may be explained as follows. In the plasma spraying process, the molten/semi-molten particles strike the substrate with a velocity of about 150–250 m/s. Upon impact, the powder particles spread in a plane parallel to the substrate and the coating is built up in which the splats are laid over one another. This splat morphology is also evidenced in cross-sectional images of the coatings, shown in Fig. 4b–d. It is assumed that during flattening of the particles most of the unstable Zr^{4+} ions (in oxygen octahedral cage) would have shifted in one crystallographic direction instead of being oriented randomly. This shifting of the Zr^{4+} ion in one direction in a large number of unit cells may have resulted in large increase in the intensity of the (002) reflection, showing a textured state. In the case of $CaZrO_3$ powder, there is a little difference between the intensities of the (200) and (002) reflections, indicating an un-textured state. To the best of authors' knowledge, the textured state of plasma sprayed $CaZrO_3$ coatings has not been reported so far.

One of the important features of ferroelectric ceramic is that it could be textured (poled) reversibly by the application of electrical loads and subsequently a positive or negative charge could be produced on the desired surface. The negative surface has a pronounced effect on the subsequent deposition of apatite in the physiological conditions [31–33]. In present study, the analysis of (200) and (002) reflections of $CaZrO_3$ powder and coatings shows that the latter are in a textured state and should have a positive or a negative charge on their surfaces. It would be interesting to know if the $CaZrO_3$ coating could be made negatively charged by applying an electrical field which, consequently, is expected to enhance apatite precipitation on this surface. Work in this area is being undertaken.

3.5. Friction and wear analysis of the substrate and coatings

The coefficient of friction and wear loss of the substrate and coatings with respect to the distance traversed were measured by a pin on disc apparatus and the results are shown in Figs. 9 and 10 respectively. The test was carried out in four steps. The distance traversed in 0–10 m, 10–35 m, 35–60 m and 60–85 m are designated as Region 1, Region 2, Region 3 and Region 4 respectively. After traversing a specified distance for each region, the instrument was stopped, debris produced by wear track was removed and the corresponding weight loss as well as coefficient of friction (COF) were recorded. For the substrate, the coefficient of friction (COF) is about 0.5 for initial 10 m (Region 1) after which it starts to decrease as the traveling distance is increased. The decrease in COF may be related to work hardening of the steel surface due to plastic deformation induced by frictional forces between the alumina ball and steel surface. For the coatings sprayed at 400 and 500 A, COF rises up to 0.5 initially and then decreases to about 0.37 during testing in Region 1. In plasma sprayed coatings well melted splats form smooth surfaces while partially/un-melted particles generate rough areas and porosity. The initial rise in COF could be linked

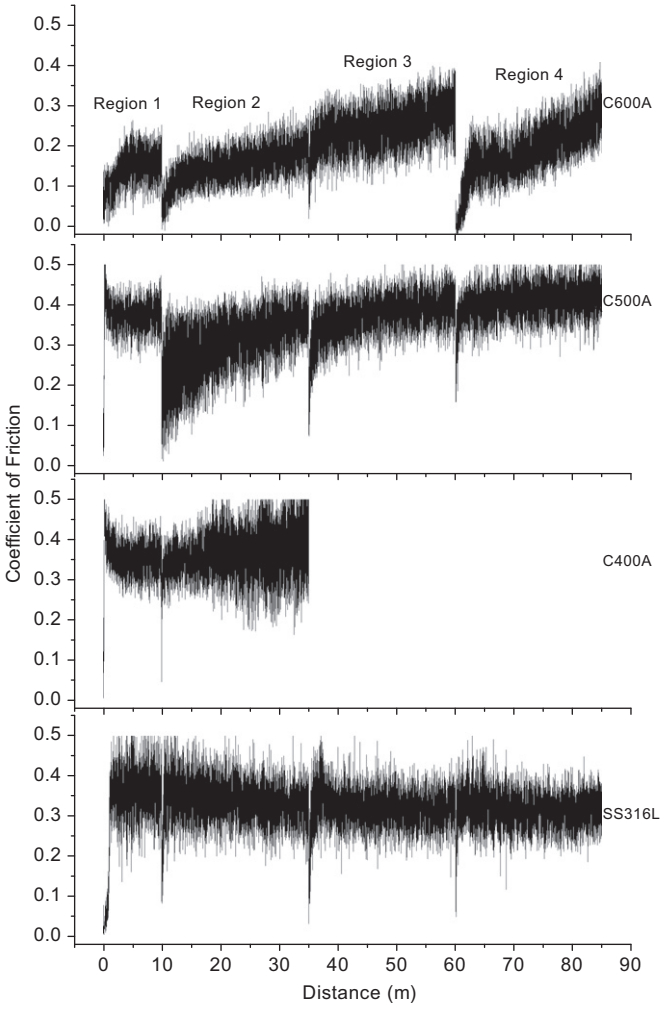

Fig. 9. Coeffficent of friction of SS316L substrate and $CaZrO_3$ coatings with respect to the distance traversed in pin on disc tribometer apparatus. From bottom to top: SS316L substrate, coating sprayed at 400 A, coating sprayed at 500 A and coating sprayed at 600 A.

to the presence of un-melted particles in these coatings. In the case of the coating sprayed at 600 A, well melted splats due to higher temperature are expected to form smooth and less porous surfaces and hence the phenomenon of initial rise and then drop in COF was not observed. These coatings, as expected, also exhibited the lowest COF values in all tested regions. It is also revealed that COF tends to increase as traveling distance is increased in each region which may be due to the generation of debris as the test is progressed.

Wear resistance of the substrate and coatings was ascertained by measuring the weight loss. In this regard, the cumulative volumetric loss is plotted against the traversed distances of 10, 35, 60 and 85 m, see Fig. 10. The maximum weight loss in Region 1 is observed for the coating deposited at 400 A which may be attributed to large porosity and less inter-splat cohesion in this coating (Fig. 4b). Its wear rate was quite high and all the deposited material disappeared while running the test in the 2nd region. This removal of material is witnessed by visual examination as well as rise in the COF (Fig. 9). After running the test up to the 2nd region, further

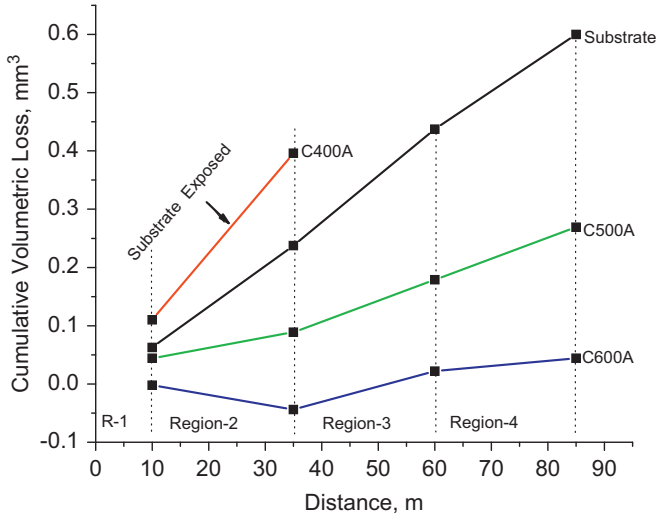

Fig. 10. Cumulative volumetric wear loss of SS316L substrate and $CaZrO_3$ coatings produced at 400, 500 and 600 A with respect to the distance traversed in pin on disc tribometer apparatus.

testing was discontinued for this coating. On the other hand, the coating deposited at the highest current (600 A) showed minimum weight loss, perhaps due to better inter-splat cohesion (Fig. 4d) and comparatively less porosity (Fig. 5). The other possible reason is higher crystallinity of this coating as revealed by reduced peak broadening in XRD data, Table 3. The cumulative volumetric loss (for traversed distance of 85 m) of the substrate was 0.6 mm^3 which is 13 times more than that of the loss suffered by $CaZrO_3$ coating sprayed at 600 A. The wear loss of the coating deposited at 500 A was in between those of the coatings that were prepared at 400 and 600 A. It made us conclude that plasma spraying of $CaZrO_3$ at 600 A is an effective way to increase the wear resistance of SS316L substrate appreciably.

4. Conclusions

The analysis of XRD reflections from the (002) and (200) planes suggests that the plasma spraying of $CaZrO_3$ produces highly textured coatings with (002) preferred orientation. The arc current was found to have a profound effect on the thickness, microstructure and wear resistance of the coatings. The wear loss of the substrate (SS316L) is 0.6 mm^3 which is 13 times higher than that of $CaZrO_3$ coating produced at 600 A. Plasma spraying of $CaZrO_3$ was not only proved to be an effective way to enhance the wear resistance of stainless steel but also showed the potential to provide a bioactive surface.

Acknowledgments

The authors are grateful to Mr. M. Munir, Mr. K. Shoaib and Mr. Atif for their help in metallographic preparation of the samples and SEM analysis.

References

[1] J.B. Park, J.D. Bronzino, Biomaterials: Principles and Applications, CRC Press, USA, 2002.
[2] G.D. Winter, Tissue reaction to metallic wear and corrosion products in human patients, Journal of Biomedical Materials Research 8 (3) (1974) 11–26.
[3] M.J. Yaszemski, Biomaterials in orthopedics, Marcel Dekker, New York, USA, 2004.
[4] C.C. Shih, C.M. Shih, Y.L. Chen, Y.Y. Su, J.S. Shih, C.F. Kwok, S.J. Lin, Growth inhibition of cultured smooth muscle cells by corrosion products of 316L stainless steel wire, Journal of Biomedical Materials Research 57 (2) (2001) 200–207.
[5] S. Morais, J. Sousa, M. Fernandes, G. Carvalho, J. De Bruijn, C. Van Blitterswijk, Effects of AISI 316L corrosion products in in vitro bone formation, Biomaterials 19 (11) (1998) 999–1008.
[6] I.B. McPhee, C.E. Swanson, Metal ion levels in patients with stainless steel spinal instrumentation, Spine 32 (18) (2007) 1963.
[7] N. Hallab, K. Merritt, J.J. Jacobs, Metal sensitivity in patients with orthopaedic implants, Journal of Bone and Joint Surgery 83 (3) (2001) 428.
[8] S. Sousa, M. Barbosa, Effect of hydroxyapatite thickness on metal ion release from Ti_6Al_4V substrates, Biomaterials 17 (4) (1996) 397–404.
[9] A.E. Porter, P. Taak, L.W. Hobbs, M.J. Coathup, G.W. Blunn, M. Spector, Bone bonding to hydroxyapatite and titanium surfaces on femoral stems retrieved from human subjects at autopsy, Biomaterials 25 (21) (2004) 5199–5208.
[10] W. Xue, S. Tao, X. Liu, X.B. Zheng, C. Ding, In vivo evaluation of plasma sprayed hydroxyapatite coatings having different crystallinity, Biomaterials 25 (3) (2004) 415–421.
[11] H.C. Gledhill, I.G. Turner, C. Doyle, In vitro dissolution behaviour of two morphologically different thermally sprayed hydroxyapatite coatings, Biomaterials 22 (7) (2001) 695–700.
[12] K. Gross, M. Babovic, Influence of abrasion on the surface characteristics of thermally sprayed hydroxyapatite coatings, Biomaterials 23 (24) (2002) 4731–4737.
[13] Y. Liu, X. Li, B. Zou, J. Chen, Z. Cai, S. Qu, M. Zhu, L. Qian, Fretting behaviors of hot-pressed electrospun hydroxyapatite/poly(*DL*-lactide) fibrous composites as potential orthopaedic implants, Tribology International 53 (2012) 124–133.
[14] Y. Fu, A.W. Batchelor, K. Khor, Fretting wear behavior of thermal sprayed hydroxyapatite coating lubricated with bovine albumin, Wear 230 (1) (1999) 98–102.
[15] Y. Fu, A.W. Batchelor, Y. Wang, K. Khor, Fretting wear behaviors of thermal sprayed hydroxyapatite (HA) coating under unlubricated conditions, Wear 217 (1) (1998) 132–139.
[16] K. Balani, R. Anderson, T. Laha, M. Andara, J. Tercero, E. Crumpler, A. Agarwal, Plasma-sprayed carbon nanotube reinforced hydroxyapatite coatings and their interaction with human osteoblasts in vitro, Biomaterials 28 (4) (2007) 618–624.
[17] K. Balani, Y. Chen, S.P. Harimkar, N.B. Dahotre, A. Agarwal, Tribological behavior of plasma-sprayed carbon nanotube-reinforced hydroxyapatite coating in physiological solution, Acta Biomaterialia 3 (6) (2007) 944–951.
[18] Y. Chen, T. Zhang, C. Gan, G. Yu, Wear studies of hydroxyapatite composite coating reinforced by carbon nanotubes, Carbon 45 (5) (2007) 998–1004.
[19] R. Singh, N.B. Dahotre, Tribology of laser modified surface of stainless steel in physiological solution, Journal of Materials Science 40 (21) (2005) 5619–5626.
[20] Y. Xie, X. Zheng, C. Ding, W. Zhai, J. Chang, H. Ji, Preparation and characterization of $CaO-ZrO_2-SiO_2$ coating for potential application in biomedicine, Journal of Thermal Spray Technology 18 (4) (2009) 678–685.
[21] G. Wang, F. Meng, C. Ding, P.K. Chu, X. Liu, Microstructure, bioactivity and osteoblast behavior of monoclinic zirconia coating with nanostructured surface, Acta Biomaterialia 6 (3) (2010) 990–1000.

[22] C. Richard, C. Kowandy, J. Landoulsi, M. Geetha, H. Ramasawmy, Corrosion and wear behavior of thermally sprayed nano ceramic coatings on commercially pure titanium and Ti–13Nb–13Zr substrates, International Journal of Refractory Metals and Hard Materials 28 (1) (2010) 115–123.
[23] J.B. Park, Bioceramics: Properties, Characterizations, and Applications, Springer–Verlag, USA, 2008.
[24] V.S. Stubican, S.P. Ray, Phase equilibria and ordering in the system ZrO_2–CaO, Journal of the American Ceramic Society 60 (11–12) (1977) 534–537.
[25] G. Wang, X. Liu, J. Gao, C. Ding, In vitro bioactivity and phase stability of plasma-sprayed nanostructured 3Y–TZP coatings, Acta Biomaterialia 5 (6) (2009) 2270–2278.
[26] G. Wang, X. Liu, C. Ding, Phase composition and in-vitro bioactivity of plasma sprayed calcia stabilized zirconia coatings, Surface and Coatings Technology 202 (24) (2008) 5824–5831.
[27] M.B. Bhatty, F.A. Khalid, A.N. Khan, Behavior of calcia-stabilized zirconia coating at high temperature, deposited by air plasma spraying system, Journal of Thermal Spray Technology 21 (1) (2012) 1–11.
[28] E. Garcia, C. Cano, T. Coyle, M. Osendi, P. Miranzo, Thermally sprayed $CaZrO_3$ coatings, Journal of Thermal Spray Technology 17 (5) (2008) 865–871.
[29] T. Yu, C. Chen, X. Chen, W. Zhu, R. Krishnan, Fabrication and characterization of perovskite $CaZrO_3$oxide thin films, Ceramics International 30 (7) (2004) 1279–1282.
[30] P. Stoch, J. Szczerba, J. Lis, D. Madej, Z. Pedzich, Crystal structure and ab initio calculations of $CaZrO_3$, Journal of the European Ceramic Society 32 (3) (2012) 665–670.
[31] T. Kobayashi, S. Nakamura, K. Yamashita, Enhanced osteobonding by negative surface charges of electrically polarized hydroxyapatite, Journal of Biomedical Materials Research 57 (4) (2001) 477–484.
[32] Y.J. Park, K.S. Hwang, J.E. Song, J.L. Ong, H. Ralph Rawls, Growth of calcium phosphate on poling treated ferroelectric $BaTiO_3$ ceramics, Biomaterials 23 (18) (2002) 3859–3864.
[33] K. Yamashita, Enhanced bioactivity of electrically poled hydroxyapatite ceramics and coatings, Materials Science Forum 426–432 (2003) 3237–3242.
[34] U. Bischoff, M. Freeman, D. Smith, M. Tuke, P. Gregson, Wear induced by motion between bone and titanium or cobalt-chrome alloys, Journal of Bone and Joint Surgery 76 (5) (1994) 713.
[35] T. Lawes, J. Scott, A. Goodship, Increased insertion torque delays pin–bone interface loosening in external fixation with tapered bone screws, Journal of Orthopaedic Trauma 18 (9) (2004) 617.
[36] J.S. Temenoff, A.G. Mikos, Biomaterials: The Intersection of Biology and Materials Science, Dorling Kindesely, India, 2009.
[37] T. Inadome, K. Hayashi, Y. Nakashima, H. Tsumura, Y. Sugioka, Comparison of bone–implant interface shear strength of hydroxyapatitecoated and aluminacoated metal implants, Journal of Biomedical Materials Research 29 (1) (1995) 19–24.
[38] W. Lee, C. Su, Y. Lee, S. Lin, T. Yang, Effects of dopant on the dielectric properties of $CaZrO_3$ ceramic sintered in a reducing atmosphere, Japanese Journal of Applied Physics 45 (2006) 5853.
[39] W. Kingery, D. Birnie, Y. Chiang, Physical Ceramics: Principles for Ceramic Science and Engineering, John Wiley and Sons, USA, 1997.
[40] G.H. Haertling, Ferroelectric ceramics: history and technology, Journal of the American Ceramic Society 82 (4) (1999) 797–818.
[41] M. Hammer, C. Monty, A. Endriss, M.J. Hoffmann, Correlation between surface texture and chemical composition in undoped, hard, and soft piezoelectric PZT ceramics, Journal of the American Ceramic Society 81 (3) (1998) 721–724.
[42] C. Bedoya, C. Muller, J.L. Baudour, V. Madigou, M. Anne, M. Roubin, Sr-doped $PbZr_{1-x}Ti_xO_3$ ceramic: structural study and field-induced reorientation of ferroelectric domains, Materials Science and Engineering B 75 (1) (2000) 43–52.
[43] S. Cheng, I.K. Lloyd, M. Kahn, Modification of surface texture by grinding and polishing lead zirconate titanate ceramics, Journal of the American Ceramic Society 75 (8) (1992) 2293–2296.